Conductance of perovskite oxide thin films and interfaces

Mubeen Dildar, I.

5

Mesoscopic transport in thin films of $La_{0.67}Sr_{0.33}MnO_3$

5.1 Introduction

The correlations among electrons in perovskite manganite thin films offer a broad framework to study their physical properties. The properties can be influenced by introducing structural defects (by strain), chemical and compositional defects (doping level, oxygen content and stoichiometry). Epitaxial thin films can behave quite different from polycrystalline thin films and single crystals. In epitaxial thin films, strain is an inherent property and it strongly affects the transport and magnetic properties [1–6]. In polycrystalline thin films, the size of grains and grain boundaries can induce subtle changes in properties of films, and microstructured and nanostructured grainy systems are well studied [7–12]. In epitaxial thin films of manganites, an area which is not much explored is the electronic transport in reduced dimensions. By reducing these to microscopic length scales, the properties can be significantly different from those in textured and epitaxial thin films. An example of this was found in (narrow band) $La_{0.7}Ca_{0.3}MnO_3$ on $SrTiO_3$, where mesoscopic bridges (typical width 1-5 μm) showed strongly non-linear behavior of the current-voltage characteristics in the temperature interval of the Metal-Insulator transition [13]. The effect was attributed to the melting of a glassy polaron state which is sensitive to the injection of electrons and which forms while going from the correlated metal to the polaronic liquid [14], in line with the details of the electronic phase diagram of (La,Ca)MnO_3 [15]. This gives rise to the question whether similar behavior can be found in a wider bandwidth material, which is the subject of this chapter.

We investigate thin films of $La_{0.7}Sr_{0.3}MnO_3$ grown on $SrTiO_3$ in which bridges of 100 μm long and 1 μm or 300 nm wide (distance between voltage contacts was 25 μm) were defined lithographically. In bridges of 1 μm, we find the current-voltage characteristics to be perfectly linear (ohmic) over the full temperature

range between 400 K and 10 K. Strong non-linearities however are observed for a 300 nm wide bridge in the temperature regime below the transition temperature. The non-linearities are present even when applying a high magnetic field of 9 T.

5.2 Experimental

Thin films of $La_{0.7}Sr_{0.3}MnO_3$ (LSMO) were deposited on $SrTiO_3$ (STO) (001) substrates using dc reactive sputtering in pure oxygen environment at pressure of 2.2 mbar. The films were deposited in the thickness range between 6 nm and 42 nm. All films were characterized by atomic force microscopy (AFM) in tapping mode after deposition. Figure 5.1a and b show morphology and height variation of a 17 nm thick film of LSMO on STO, called LS32. The roughness of the film is 2.1 nm and it has step-height variations of the order of a unit cell (0.4 nm). Figure 5.1c,d show the surface morphology and the height variation perpendicular to the terraces of a 6 nm-thick film of LSMO on STO, called LS41. The step variation is again 0.4 nm but the roughness of film is low, 0.4 nm, a bit smoother than the thicker film in Figure 5.1a.

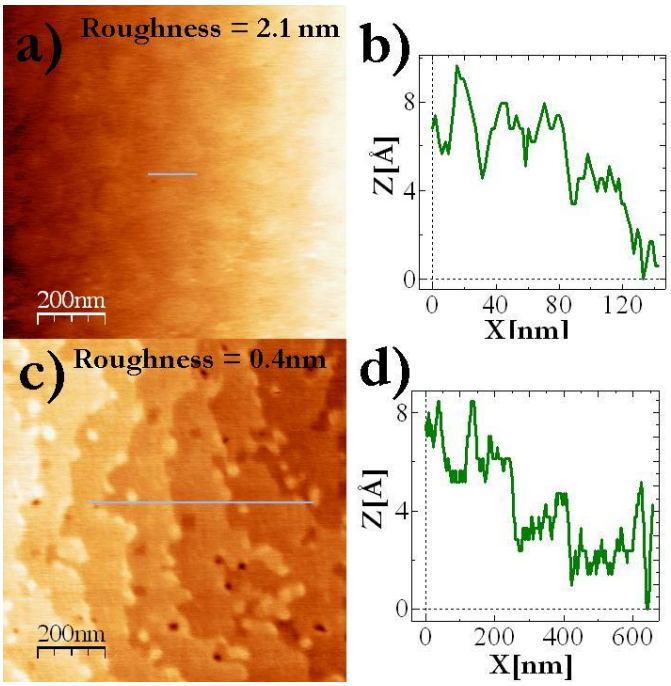

Figure 5.1: Surface morphology of (a) a 17 nm film of LSMO on STO (LS32), (b) height variation of (a) along the drawn line, (c) a 6 nm film of LSMO on STO (LS41), (d) height variation of (c) along the drawn line.

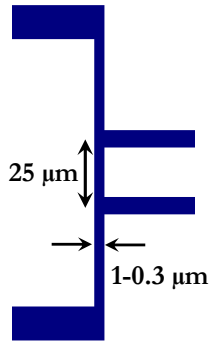

Figure 5.2: The structure of patterned bridges of LSMO on STO. The length of the bridge is 100 μm and the distance between voltage contacts is 25 μm.

The film thickness was measured by x-ray reflectivity, using Cu-Kα radiation. The lattice mismatch between bulk LSMO (a_c = 0.3873 nm) thin films and single crystal STO substrates (001) (a_c = 0.3905 nm) is -0.82 %. Thin films grown on STO are therefore strained. The strain gradually relaxes with increasing thickness.

The films were patterned using e-beam lithographic technique. A three-step process was used to pattern LSMO microbridges of 1 μm and 300 nm wide with Au contact pads. A typical structured pattern for the microbridges is shown in Figure 5.2. In the first step, gold markers were written to have a better contrast with STO substrates. A bilayer of PMMA/MMA was spun on top of the samples and baked at 180°C/120°C respectively for 90/90 seconds. Then markers were written with e-beam. After developing, the samples were sputtered with gold and the lift-off process was accomplished. In the second step, a negative resist (MaN2405) was spun onto the sample, and baked at 90° C for 10 minutes. Then the chip of LSMO was written with e-beam with Au markers as reference. After developing, the sample was etched with wet etching. The chemicals used for wet etching and their respective quantities were (H_2O: HF: HCl: HNO_3 = 25: 1: 1: 1). The etch rate was 2 nm per second for the LSMO thin films. Lastly, the first step was repeated for making Au contacts. A physical properties measurement system (PPMS) was used for the temperature and field control. External current sources and voltmeters were used for the transport measurements of unstructured and structured thin films and for the current-voltages characteristics.

5.3 Results

1 μm wide bridges

Figure 5.3 shows the transport properties of two thin films of LSMO on STO of (a) 17 nm and (b) 6 nm measured with 1 μA current. The unstructured samples

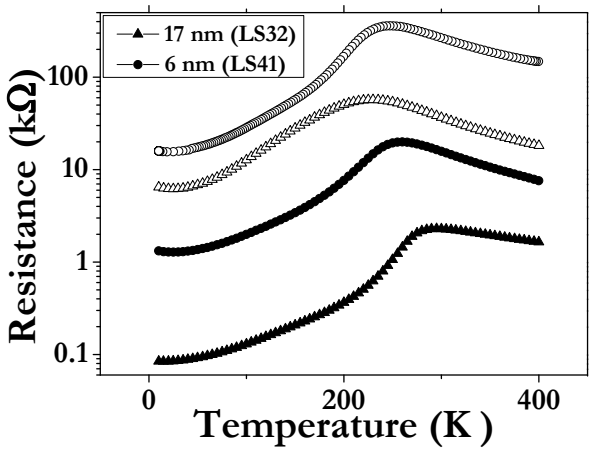

Figure 5.3: Resistance versus temperature behavior for two films of LSMO on STO (a) a 17 nm film (LS32) (b) a 6 nm film (LS41). Closed symbols are for unstructured films. Open symbols denote R (T) for 1 μm wide bridges. The measurement current is 1 μA for all films shown here.

have a transition temperature of about 290 K and 250 K as compared to the bulk LSMO 370 K. Both films are strained as measured by XRD. The strain reduces the transition temperature by about 100 K. There is not much difference between unstructured and structured films except that the low-temperature resistance is increased about 100 times for the 17 nm film and only about 10 times for the 6 nm film, although the resistance of the 17 nm film is still lower than that of the 6 nm film.

To further explore the behavior of LSMO on micrometer scales, we measured the current-voltage characteristics at different temperatures for thin films of LSMO between 6 nm and 42 nm. For all 1 μm bridges, we observe a perfect linear behavior while measuring IV-curves for the whole temperature range. We show in Figure 5.4 the IV curves for a 17 nm thin film of LSMO/STO for a 1 μm wide bridge. The data are presented as current density, where the cross-section is taken as 17 nm$\times$1 μm. The same behavior is found for the other films, including the 6 nm thick film (LS41). The derivatives of these curves are shown in Figure 5.5. The non-linearities found in LCMO microbridges [13] are clearly not found here.

300 nm wide bridges

Going from a width of 1 μm to a bridge of 300 nm, the behavior changes quite drastically. Figure 5.6 shows the R(T) behavior of three films of LSMO on STO. The 42 nm thick film (LS38) does not show unusual behavior, with a peak temperature above 300 K both for structured and unstructured ones. The 10 nm thin film

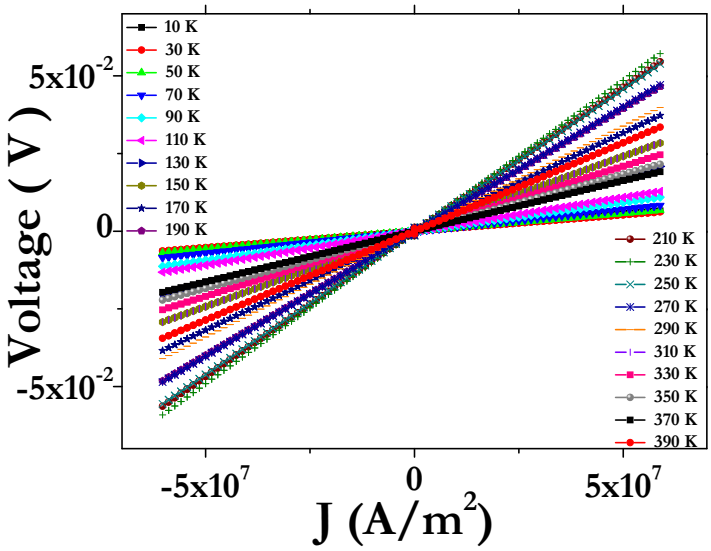

Figure 5.4: Current voltage characteristics for a 17 nm thin film of LSMO on STO (LS32) with a 1 μm wide bridge. The current density was calculated from the 17 nm×1 μm cross-section of the bridge.

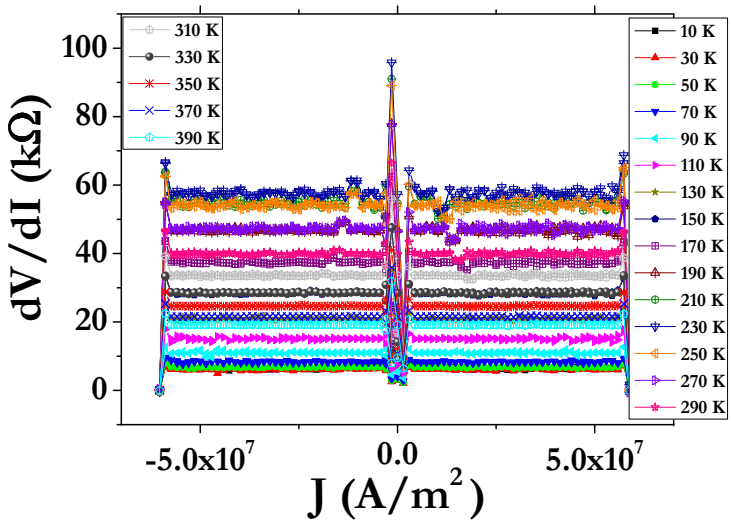

Figure 5.5: Derivatives of current-voltage curves for a 17 nm thin film of LSMO on STO (LS32) for the 1 μm wide bridge shown in Figure 5.4. The peak structure around zero current is due to a discontinuity in the source current.

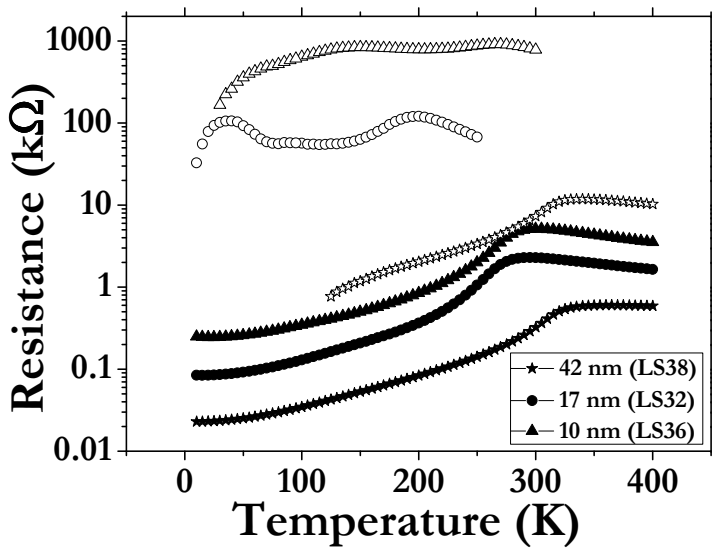

Figure 5.6: Temperature dependence of the resistance for 300 nm wide bridge of LSMO thin films with different thickness of 42 nm (LS38), 17 nm (LS32) and 10 nm (LS36). The unstructured films are shown with filled symbols and the 300 nm bridges films are shown with open symbols. The measurement current is 1 μA for all films shown here except for the unstructured LS38, measuring current is 10 μA.

(LS36) shows a small upturn at low temperature and the peak temperature goes down to 250 K while the unstructured film has T_p around 300 K. The 17 nm thin film (LS32) has two resistance peaks. One lies at 185 K which can be considered as T_p; the peak around 50 K does not have a straightforward origin. Note that the resistance of the 10 nm film is about an order of magnitude larger than the resistance of the 17 nm film over most of the temperature range.

We further explored the characteristic in 300 nm wide bridges by measuring IV curves. The 10 nm film (LS36) with the 300 nm wide bridge is shown in Figure 5.7. Here, we observe strong nonlinearities which start around 40 K and continue until 190 K. The derivatives of such IV curves are shown in Figure 5.8 which clearly divide the nonlinear behavior into three different regions. These effects are not found in the 42 nm film with the 300 nm bridge. The first region is between 10 K to 40 K (Figure 5.8a) where ohmic behavior can be seen. The second region between 50 K and 150 K (Figure 5.8b) shows a strong peak at the zero bias, indicating a strong nonlinear behavior. In the third region which starts around 200 K, the nonlinear behavior becomes shallow and after T_p, nonlinearities disappear fully. We see same trend of nonlinearity in 17 nm thin film of LSMO for the 300 nm wide bridge.

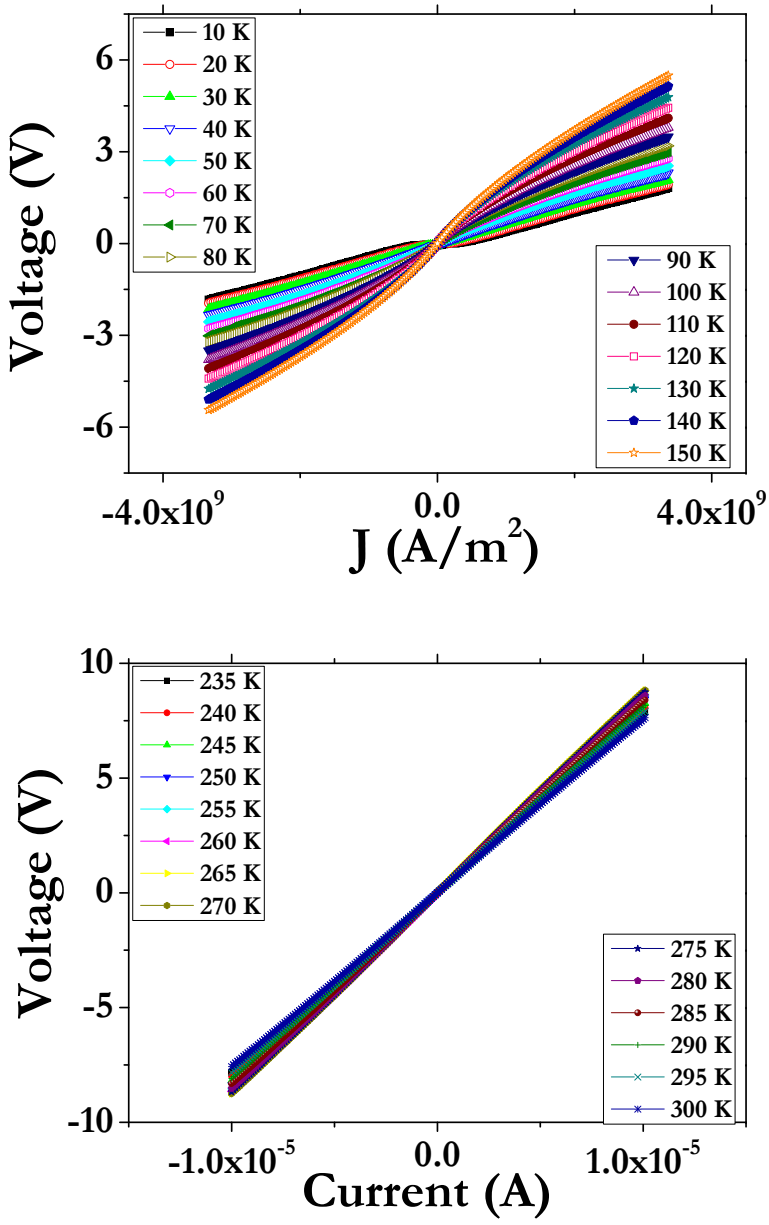

Figure 5.7: Current voltage characteristics for a 10 nm thin film of LSMO on STO (LS36) for 300 nm wide bridge. The current density was calculated from the 10 nm×300 nm cross-section of the bridge.

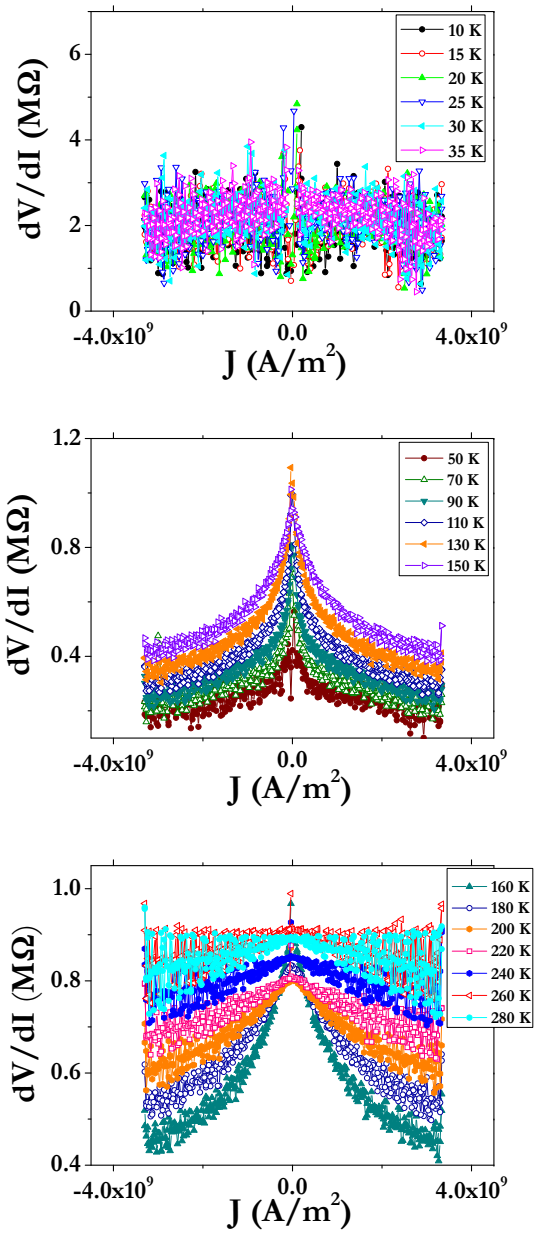

Figure 5.8: Derivatives of some of current-voltage curves shown in Figure 5.7 for the 10 nm thin film of LSMO on STO (LS36) with a 300 nm wide bridge. (a) first region 10 K to 40 K, fully linear (b) second region between 50 K and 150 K, strongly nonlinear (c) third region after 180 K, slightly nonlinear and nonlinearity disappears with increasing temperature.

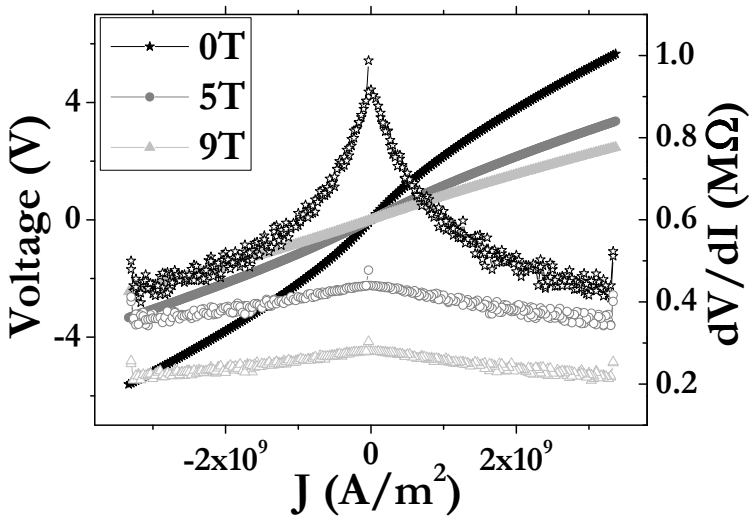

Figure 5.9: Effect of magnetic field on 300 nm wide bridge of a 10 nm film (LS36) of LSMO on STO at 155 K. Left axis shows the voltage and right axis is for the derivatives taken from the IVs curves.

The effect of an applied magnetic field on these IV curves is shown in Figure 5.9 for the 10 nm (LS36) film at 155 K. The strongest effect was obtained at 0 T. The left axis shows IV-curves and derivatives are shown on right axis. The nonlinear behavior is strongly reduced by applying a high magnetic field.

The nonlinear effects can also be displayed as R(T) at different currents as shown in Figure 5.10. The current has no significant effects on a 42 nm thick film of LSMO but for thin films, increasing the current decreases the resistance. These effects are consistently seen in thin films structured into 300 nm wide bridges. Looking at Figure 5.10c (the 10 nm film again), it is also here clear that the nonlinear behavior is strongest in the region of 50 K to 150 K, where different current give a significantly different resistance.

5.4 Discussion

Nonlinear IV characteristics at temperatures below the IM transition have been observed in two types of circumstances. They were found in oxygen-deficient films, and they were observed across artificially fabricated grain boundaries (GB). In the latter case, it is basically a tunneling phenomenon. In particular Klein *et al.* showed that a series of such GB's could lead to an R(T) with two peaks [8]. Moreover, they were able to fit their IV curves to a model suggested by Glazman and Matveev, in which the current is carried by a multistep tunneling process

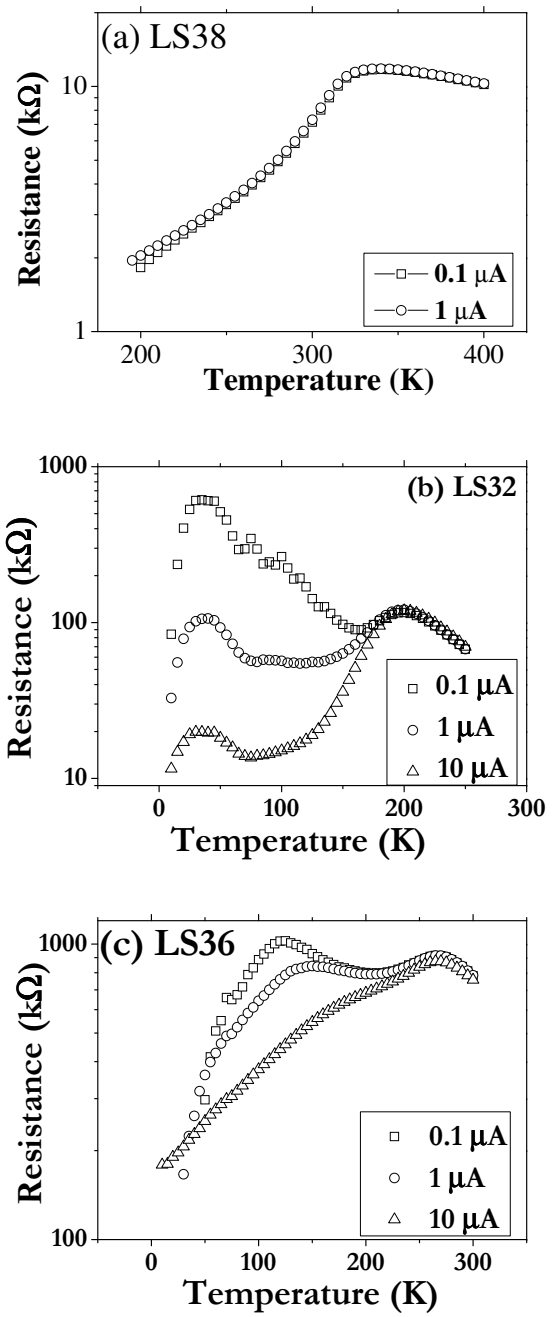

Figure 5.10: Temperature dependence of resistance for 300 nm wide bridge of LSMO films under different dc currents (a) a 42 nm film (LS38) (b) a 17 nm film (LS32) (c) a 10 nm film (LS36).

Sample ID	d_{LSMO} (nm)	J (A/m^2) (1 μm, 1 μA)	J (A/m^2) (300 nm, 10 μA)
LS38	42	2.4×10^7	8×10^8
LS32	17	5.9×10^7	2×10^9
LS36	10	1×10^8	3×10^9
LS41	6	1.7×10^8	6×10^9

Table 5.1: Current densities for thin films of LSMO calculated for 1 μm and 300 nm wide bridges at currents of 1 μA and 10 μA respectively. Given are the sample ID, thickness of LSMO d_{LSMO} (nm), current density J (A/m^2) for 1 μm bridge and 300 nm wide bridges.

involving 1,2,3...n localized states. This leads to a voltage-dependent conductance $G(V) = G_o + G_1 + G_2\ V^{4/3} + G_3\ V^{5/2}$ with $I = G\ (V)\ V$. Note that for simple tunneling one would expect something like $G\ (V) = a + b\ V^2$. Figure 5.11 shows what the GB expression would look like for the data taken on the 10 nm film at 155 K, using the $G_o + G_1 + G_2$ terms. It is clear that the measured behavior is too shallow for a tunneling description. That leaves oxygen vacancies, as a possible candidate. This case was studied by Liu *et al.* on thin films of $La_{0.7}Ca_{0.3}MnO_3$, which were annealed to different degrees in order to remove oxygen [22]. They basically found a spike-like voltage dependent conductance, similar to the behavior shown in Figure 5.8b, for slightly oxygen deficient material; or more parabolic behavior, reminiscent of tunneling, for the highly oxygen deficient films. Our case of the 300 nm bridges resembles the slight oxygen deficiency, and this is also the case for the behavior in a magnetic field, where the nonlinear behavior disappears. The data therefore suggest that the 300 nm bridges are significantly more oxygen-deficient than the 1 μm bridges. This could well be the result of the lithographic structuring process. If that leads to a depleted zone with an extension of half the bridge width , the 1 μm bridges would not be affected. That leaves the question why the resistance decreases so strongly with the increasing current or voltage. Following ref. [21] we would argue that oxygen loss leads to a decrease of the amount of Mn^{+4}, and therefore locally to lower T_c's. The bridge then is a mixture of material with different T_c's, and the nonlinearities disappear when all regions have become metallic, around 50 K. Using the results of Dörr *et al.* [21], this suggests that the Mn^{+4} concentration has decreased to 0.2, corresponding to an oxygen loss $\delta = 0.05$ in the formula $La_{0.7}Sr_{0.3}MnO_{3-\delta}$.

The data also indicate, however, that the current can drive the mixed regions metallic. A possible mechanism here is that carriers are released which were initially trapped by the disorder. An oxygen defect produces extra Mn^{+3} ions with the tendency of a local Jahn - Teller deformation as well as antiferromagnetic correlations. The current is supposed to be spin polarized, and it has been conjectured that spin torque effects could flip the spin of Mn^{+3} ion and free that charge. In homogeneous manganite systems this would mean that a current could enhance T_c, which has never been observed. This need not be surprising, since the current densities for generating spin torque effects are very high. In typical experiments

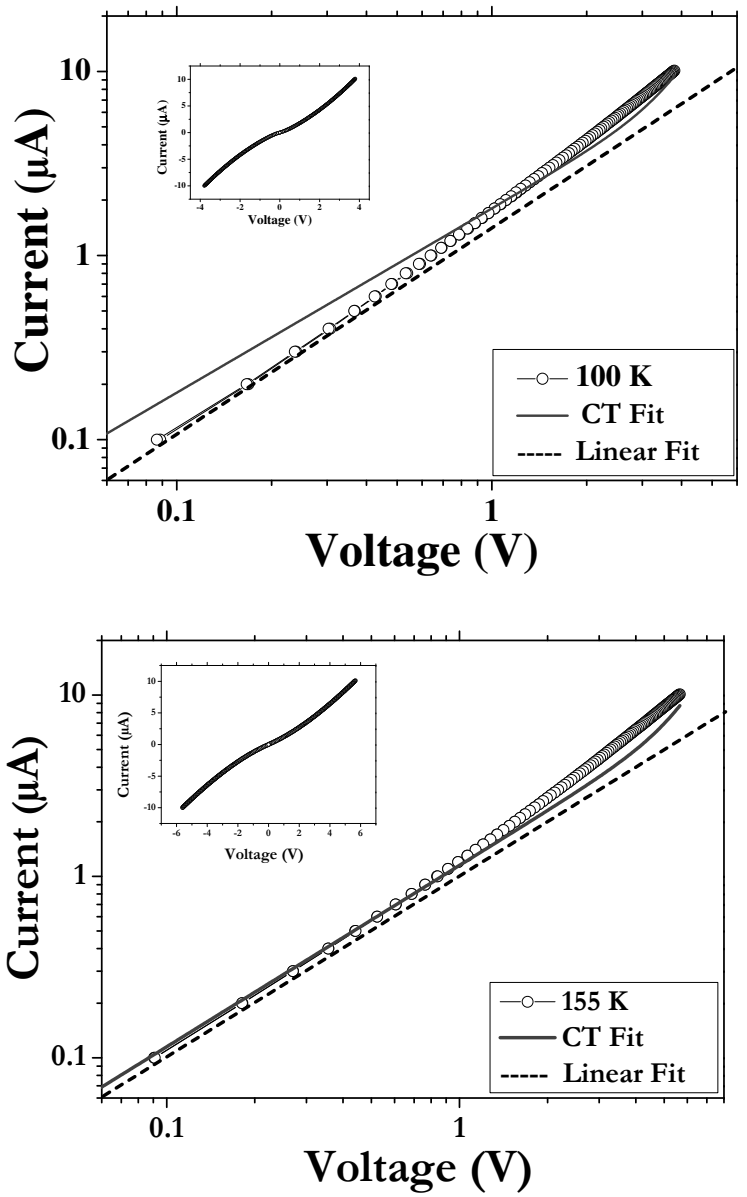

Figure 5.11: (a) Current-voltage curves for a 10 nm LSMO on STO at (a) 100 K (b) 155 K. The curves are plotted on a double logarithmic scale, the dark grey line represents the least square fit to the CT (conductance tunneling) fit, I = G (V) V where $G(V) = G_o + G_1 + G_2\ V^{4/3} + G_3\ V^{5/2}$ and the black dashed line is the linear fit, the insets show the IV curves on linear scale.

involving magnetic nanopillars, the values are of the order of 10^{11} A/m^2 [24]. In our case, however, the system is manifestly inhomogeneous, which means filamentary current distribution, and the current densities are very large. Table 5.1 shows that, when the full bridge area is taken into account, the current density at 10 μA is 3×10^9 A/m^2. This is a conservative estimate, since we know from the experiments described in chapter 4 that a dead layer is likely to occur and the 10 nm layer is probably rather a 5 nm layer, so that the order of magnitude is at least 10^{10} A/m^2.

A final point to address is the behavior of the 42 nm film, which behaves quite like the bulk material. Apparently, oxygen depletion is not as strong for the thinner film as it is for the thicker one. The reason for this is not yet clear.

5.5 Conclusion

We conclude that thin films of LSMO lose some oxygen locally in 300 nm wide bridges which results in highly nonlinear behavior in IV curves at intermediate temperatures. The effect is only seen in thin films less than 18 nm. The effect appears to be due to inhomogeneities in the oxygen distribution, and is therefore different from the effects found in LCMO bridges, where a homogeneous glassy state was posed to occur. The present study gives an opportunity to explore the additional effects in physical properties of manganites on microscopic scales.

Bibliography

[1] J. Aarts, S. Freisem, R. Hendrikx, and H.W. Zandbergen, Appl. Phys. Lett. **72**, 2975 (1998).

[2] Y. Konishi, Z. Fang. M. Izumi, T.Mamako. M. Kasai, H. Kuwahara, M. kawasaki, K. Terakura and Y. Tokura, J. Phys. Soc. Jpn. **68**, 3790 (1999).

[3] Z. Fang, I.V. Solovyev, and K. Terakura, Phys. Rev. Lett. **84**, 3169 (2000).

[4] M. Bibes, Ll. Balcells, S. Valencia, J. Fontcuberta, M. Wojcik, E. Jedryka, and S. Nadolski, Phys. Rev. Lett. **87**, 067210 (2001).

[5] Z.Q. Yang, R. Hendrikx, J. Aarts, Y.L. Qin, and H.W. Zandbergen, Phys. Rev. B **70**, 174111 (2004).

[6] M. Huijben, L.W. Martin, Y.-H. Chu, M.B. Holcomb, P. Yu, G. Rijnders, D.H.A. Blank, and R. Ramesh, Phys. Rev. B **78**, 094413 (2008).

[7] A. Gupta, G.Q. Gong, G. Xiao, P.R. Duncombe, P. Lecoeur, P. Trouilloud, Y.Y. Wang, V.P. Dravid, J.Z. Sun, Phys. Rev. B **54**, R15629 (1996).

[8] J. Klein, C. Hofener, S. Uhlenbruck, L. Alff, B. Buchner, and G. Gross, Euro. Phys. Lett. **47**, 371 (1999).

[9] A.M.H. Gosnet, J. Wolfman, B. Mercey, C. Simon, P. Leoceur, M. Korzenski, M. Hervieu, R. Desfeux, G. Baldinozzi, J. Appl. Phys. **88**, 4257 (2000).

[10] Y. Fu, Appl. Phys. Lett. **77**, 118 (2000).

[11] A.D. Andres, J. Rubio, G. Castro, S. Taboada, J.L. Martinez, J.M. Colino, J. Appl. Phys. **83**, 713 (2003).

[12] B. Ghosh, S. Kar, L.K. Brar, A.K. Raychaudhuri, J. Appl Phys. **98**, 094302 (2005).

[13] C. Beekman, J. Zaanen, and J. Aarts, Phys. Rev. B **83**, 235128 (2011).

[14] V. Markovich, E.S. Vlakhov, Y. Yuzhelevskii, B. Blagoev, K.A. Nenkov, and G. Gorodetsky, Phys. Rev. Lett. **72**, 134414 (2005).

[15] Y. Tokura, Colossal Magnetoresistive Oxides, Vol. **2**, Gordon & Breach Science publishers, 2000.

[16] J. Gao, S.Q. Shen, T.K. Li, and J.R. Sun, Appl. Phys. Lett. **82**, 4732 (2003).

[17] C. Barone, C. Adamo, A. Galdi, P. Orgiani, A.Y. Petrov, O. Quarnta, L. Maritato, and S. Pagano, Phys. Rev. B **75**, 174431 (2007).

[18] T. Wu, S.B. Ogale, J.E. Garrison, B. Nagaraj, A. Biswas, Z. Chen, R.L. Greene, R. Ramesh, T. Venkatesan, and A.J. Millis, Phys. Rev. Lett. **86**, 5998 (2001).

[19] M. Fäth, S. Freisem, A.A. Menovsky, Y. Tomioka, J. Aarts, and J.A. Mydosh, Science **285**, 1540 (1999).

[20] L. Bery, Phys. Rev. B **75**, 104423 (2007).

[21] K. Dörr, J.M. De. Teresa, K-H. Müller, D. Eckert, T. Walter, E. Vlakhov, K. Nenkov, and L. Schultz, J. Phys. Condens. Matter **12**, 7099 (2000).

[22] S.J. Liu, J.Y. Juang, J.-Y. Lin, K.H. Wu, T.M. Uen, and Y.S. Gou, J. Appl. Phys. **103**, 023917 (2008).

[23] L.I. Glazman, and K.A. Matveev, Sov. Phys. JETP **67**, 1276 (1988).

[24] J.A. Katine, F.J. Albert, R.A. Buhrman, E.B. Myers and D.C. Ralph, Phys. Rev. Lett. **84**, 8149 (2000).